A treatise on InSAR geometry and 3D displacement estimation

Wietske S. Brouwer and Ramon F. Hanssen, *Senior Member, IEEE*

***Abstract*—The estimation of displacement vectors for (objects on) the Earth's surface using satellite InSAR requires geometric transformations of the observables based on orbital viewing geometries. Usually, there are insufficient viewing geometries available for full 3D reconstruction, leading to non-unique solutions. Currently, there is no standardized approach to deal with this problem, resulting in products that are based on haphazard and/or oversimplified assumptions with biased estimates and reduced interpretability. Here we show that a clear definition of—and subsequent adherence to—enabling conditions guarantees the validity and quality of displacement vector estimates leading to standardized interferometric products with improved interpretability. We introduce the concept of the null line as a key metric for InSAR geometry and bias estimation, assess its impact and orientation for all positions on Earth, and propose a novel reference system that is inherently unbiased. We evaluate current operational practice, leading to a taxonomy of frequently encountered misconceptions and to recommendations for InSAR product generation and interpretation. We also propose new subscript notation to uniquely distinguish different projection and decomposition products. Our propositions contribute to further standardization of InSAR product definition, improved map annotation, and robust interpretability.**

***Index Terms*—InSAR, surface displacements, line-of-sight, decomposition, null line, projection, solution space**

I. Introduction

IT is well known that InSAR phase observations are only sensitive to the projection of the 3D displacement vector onto the radar line-of-sight (LoS) direction, along a plane orthogonal to the LoS [1]. This projection, d_{LoS}, in a Cartesian east, north, up (ENU) coordinate system is described by

$$d_{\text{LoS}} = P_{\text{LoS}^\perp}\, d_{\text{ENU}}, \tag{1}$$

where $P_{\text{LoS}^\perp} = [\sin\theta \sin\alpha_d, \sin\theta \cos\alpha_d, \cos\theta]$ is the orthogonal projector onto the line of sight, $d_{\text{ENU}} = [d_e, d_n, d_u]^T$ is the 3D displacement vector in east, north, and up direction, respectively, θ is the incidence angle towards the radar, and α_d is the azimuth of the zero-Doppler plane at the position of the target, in the direction towards the satellite, see Fig. 1. In the early years of InSAR, one viewing geometry was used for estimating displacements [2], [3], [4]. However, the possibility to combine ascending and descending orbits imaging the same area of interest triggered attempts to estimate the 3D displacement vectors [5], [6], [7], [8]. Evidently, to estimate the full 3D displacement vector, one would need three independent viewing geometries, using three different $P_{\text{LoS}^\perp}$ projectors forming a full rank matrix with a low condition number [9]. Yet, while the near-polar orbits of contemporary SAR missions cause an imaging geometry that differs significantly between ascending and descending orbits, it does not for adjacent tracks [6], [10]. As a result, the sensitivity is rather unbalanced for the three Cartesian directions [1]. Moreover, in many practical situations only two LoS observation geometries are available, i.e., ascending and descending, resulting in an underdetermined system with an infinite amount of possible solutions.

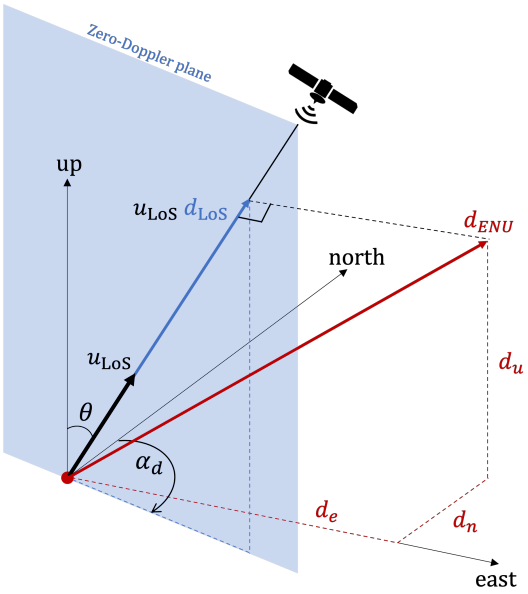

Fig. 1. Schematic overview of the projection of the displacement vector d_{ENU} onto the LoS direction of a satellite in a descending orbit. The LoS direction of the satellite can be described with two angles: the incidence angle θ and the azimuth of the zero-Doppler plane α_d. Those angles are described at the position of the target.

The way in which this problem is typically handled in InSAR literature and operational practice often leads to biased estimation, and requires more standardization and mathematical and semantic rigor. Concepts such as *decomposition* and *projection* need to be distinguished, substantiated assumptions that can serve as boundary conditions, need to be explicitly stated. In this study, we provide a comprehensive overview of the topic, proposing necessary terminology and estimation techniques for the inverse problem. We discuss the limitations of the decomposition and propose a standardized approach. In Sec. II we give an overarching mathematical framework rooted in linear algebra, building on previous work by [1], [6], [7] and [8]. In Sec. III we explicitly state the conditions for a successful inversion, and in Sec. IV we introduce of

W.S. Brouwer and R.F. Hanssen are with the Department of Geoscience and Remote Sensing, Delft University of Technology, Delft, 2628 CN, The Netherlands (email: w.s.brouwer@tudelft.nl, r.f.hanssen@tudelft.nl).

the concept of the *null line*, which can be used to propose a coordinate system that is intrinsically unbiased. Using these concepts, we evaluate current practice and identify three types of typical geometric flaws encountered in literature in Sec. V and provide recommendations for InSAR product generation and interpretation in Sec. VI.

II. Theory

To solve for the full 3D displacement vector, several conditions (all necessary but individually not sufficient) need to be satisfied. Therefore, we first review the relevant InSAR geometry and the forward model in Sec. II-A and II-B, respectively.

A. The viewing geometry

The estimated relative displacements resulting from InSAR parameter estimation are projections of the 3D displacement vector onto the line-of-sight (LoS) direction defined at the position of the target, see Eq. (1). The LoS direction depends on the viewing geometry towards the satellite. Therefore, the LoS direction is described using two angles:[1] the azimuth of the zero-Doppler plane at the Earth's surface, α_d, and the incidence angle, θ, see Fig. 1.

1) Azimuth of the zero-Doppler plane: Most SAR satellites operate from retrograde sun-synchronous near-polar orbits. While the orbital plane of the satellite has a fixed inclination, the satellite has a time-varying orbital heading α_h, which is the angle between the velocity vector of the satellite and the geometrical north. Most contemporary SAR observations are taken at zero-Doppler [1], which defines the zero-Doppler plane (ZDP): the plane perpendicular to the heading of the satellite. Thus, the LoS vector lies in the ZDP.

The heading, α_h and the orientation of the ZDP—in a satellite-centered coordinate frame—are different from the direction of the velocity vector and the azimuth of the ZDP, α_d, in a target-centered coordinate frame on the Earth's surface, see Fig. 2. This effect is caused by the side-looking geometry of the SAR and the non-parallel nature (convergence) of the Earth's meridians. Additionally, the azimuth of the zero-Doppler plane is range dependent. These effects are relevant when computing the viewing geometry. Thus, the projector $P_{\text{LoS}^\perp}$ should be defined usig α_d rather than using α_h.

2) Incidence angle: The incidence angle, θ, refers to the nominal (ellipsoidal) incidence angle, i.e., the angle between the normal vector on the local ellipsoid, at the position of the target, and the line of sight towards the satellite in the ZDP. The incidence angle differs from the satellite look angle θ_l, which is the angle between the LoS direction and the nadir of the satellite sensor, due to the curvature of the Earth, see Fig. 3. Moreover, the nominal incidence angle varies with the range direction resulting in different incidence angles for different targets (pixels) within the same image [11].[2]

[1]These angles are not to be confused with the heading angle and look angle of the satellite, respectively, as we will discuss below.

[2]For example, the incidence angle for the Sentinel-1 Interferometric Wide swath varies between 29° and 46°.

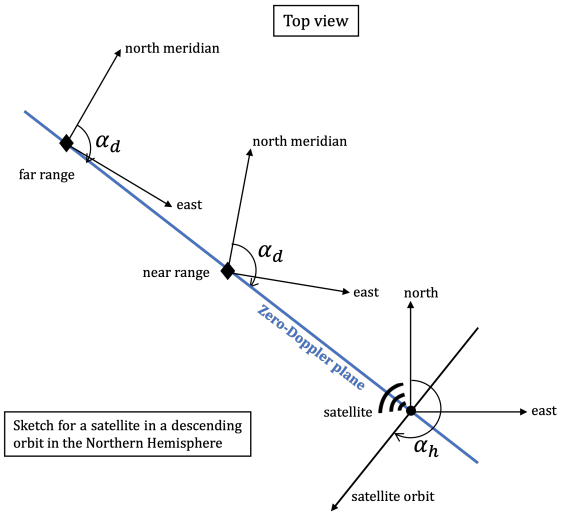

Fig. 2. Two targets on Earth (black diamonds) observed from a satellite (black dot) in a descending orbit in the Northern Hemisphere. The velocity vector of the satellite has azimuth angle α_h with respect to the geographical north. Due to the meridian convergence, the north direction at the Earth's surface at near range (nr) differs from the north direction at far range (fr). Thus, the orientation of the zero-Doppler plane (in blue) depends on the target position in range, i.e., $\alpha_{d,\text{nr}} \neq \alpha_{d,\text{fr}}$.

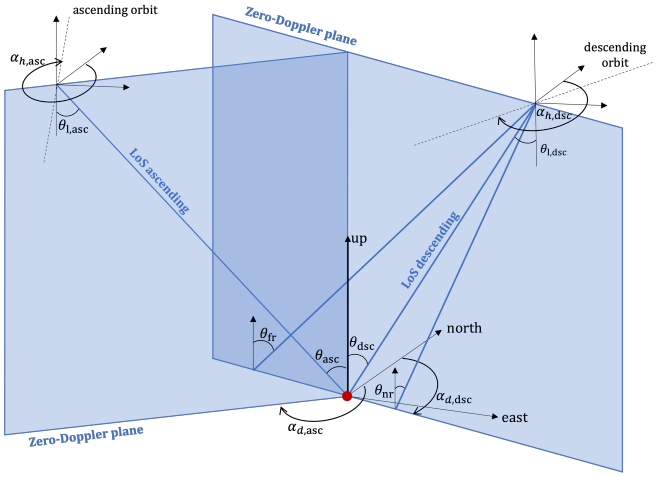

Fig. 3. Schematic overview of the viewing geometry. The heading angles $\alpha_{h,\text{asc}}$ and $\alpha_{h,\text{dsc}}$ are the azimuth angles of the velocity vectors of the satellites with respect to the geometrical north. α_d is the azimuth of the zero-Doppler plane, at the position of the target (red dot), in the direction towards the satellite. The incidence angle is the angle between the LoS vector and the local zenith and varies from near to far range, i.e., $\theta_{\text{fr}} > \theta_{\text{nr}}$.

As both the incidence angle and azimuth of the ZDP are range dependent, they are correlated. Due to the meridian convergence, the orientation of the target-centered coordinate system with respect to the satellite-centered coordinate system differs from near to far range, see Fig. 2. Therefore, α_d is range dependent, i.e., $\alpha_{d,\text{nr}} \neq \alpha_{d,\text{fr}}$ where nr and fr represent near and far range, respectively. The interdependence between θ and α_d is visualized in Fig. 4 for Sentinel-1 acquisitions at sea level with a varying latitude and an arbitrary longitude, here 40°E, for all available ascending (top) and descending (bottom) acquisitions [12].

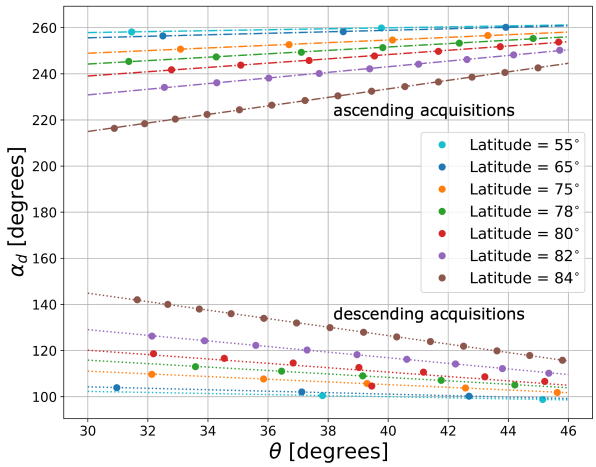

Fig. 4. Viewing geometries towards all visible Sentinel-1 swaths (circular marks), for different latitudes on the Northern Hemisphere, at an arbitrary longitude 40°E. For ascending acquisitions (top), the correlation is positive, for descending acquisitions (bottom), it is negative. For the Southern Hemisphere this is reversed.

B. Forward model

The displacement d_{LoS} of a target observed from a satellite is the orthogonal projection of d_{ENU} onto the LoS direction, see Eq. (1). We refer to this as a *forced* projection, as it is an implicit autonomous operation. As Eq. (1) represents the displacement as a scalar, it requires a directional unit vector to specify its direction, i.e.,

$$d_{\text{LoS}}\, \mathrm{u}_{\text{LoS}} = \text{diag}(P_{\text{LoS}^\perp})\, d_{\text{ENU}}, \tag{2}$$

where u_{LoS} is the LoS unit vector, defined as

$$\mathrm{u}_{\text{LoS}} = \begin{bmatrix} \mathrm{u}_1 \\ \mathrm{u}_2 \\ \mathrm{u}_3 \end{bmatrix} = \begin{bmatrix} \sin\theta \sin\alpha_d \\ \sin\theta \cos\alpha_d \\ \cos\theta \end{bmatrix}, \tag{3}$$

and $P_{\text{LoS}^\perp}$ refers to a projector *onto* the LoS, *along* a plane orthogonal to the LoS unit vector, see Eq. (1). The LoS unit vector has its origin at the target, i.e., motion towards the satellite yields a decrease in slant range.

Given this forward model, we evaluate the inverse model to estimate the displacement parameters and discuss the necessary and sufficient conditions for this estimation.

III. Conditions for the Inverse Model

Estimated LoS displacements are one-dimensional and may be difficult to interpret by end-users, who are mostly interested in the 'real' (3D) displacements. This requires a *decomposition* of the LoS displacements, i.e., the inverse problem [13]. The functional relation of Eq. (1) is therefore extended to a full mathematical model, including

$$E\{\underbrace{\begin{bmatrix} \underline{d}^{(1)}_{\text{LoS}} \\ \underline{d}^{(2)}_{\text{LoS}} \\ \vdots \\ \underline{d}^{(m)}_{\text{LoS}} \end{bmatrix}}_{\underline{y}}\} = \underbrace{\begin{bmatrix} P^{(1)}_{\text{LoS}^\perp} \\ P^{(2)}_{\text{LoS}^\perp} \\ \vdots \\ P^{(m)}_{\text{LoS}^\perp} \end{bmatrix}}_{A} \underbrace{\begin{bmatrix} d_e \\ d_n \\ d_u \end{bmatrix}}_{x}, \text{ and} \tag{4}$$

$$D\{\underbrace{\begin{bmatrix} \underline{d}^{(1)}_{\text{LoS}} \\ \underline{d}^{(2)}_{\text{LoS}} \\ \vdots \\ \underline{d}^{(m)}_{\text{LoS}} \end{bmatrix}}_{\underline{y}}\} = \underbrace{\begin{bmatrix} Q_{\text{LoS},1} & 0 & \dots & 0 \\ 0 & Q_{\text{LoS},2} & \dots & 0 \\ \vdots & \vdots & \ddots & \vdots \\ 0 & 0 & \dots & Q_{\text{LoS},m} \end{bmatrix}}_{Q_y}, \tag{5}$$

where $\underline{y}$ is the observation vector, containing vectors $\underline{d}^{(1)}_{\text{LoS}}$ until $\underline{d}^{(m)}_{\text{LoS}}$, which are m sets of LoS displacement observations. The underline indicates the stochastic nature of the vector. Each vector $\underline{d}^{(i)}_{\text{LoS}}$ represents an independent viewing geometry (orbital position), and contains the observations from all scatterers within the same region of uniform motion (RUM, discussed in Sec. III-B), which we henceforth term a *set*. The size of each set can be different since the number of available coherent scatterers within a RUM can differ. $E\{.\}$ and $D\{.\}$ are the expectation and dispersion operator, respectively, and $Q_{\text{LoS},i}$ is the variance-covariance matrix of an independent observation set. When $\underline{d}^{(i)}_{\text{LoS}}$ has size $p \times 1$ there are p scatterers within the RUM for that particular viewing geometry. $Q_{\text{LoS},i}$ is a $p \times p$ diagonal matrix with the variances of the LoS observations on the diagonal. For small RUMs (< 100 m) the off-diagonal elements are equal to zero, since all observations represent different uncorrelated physical scatterers acquired at different times and the atmospheric delay can be considered as constant for all scatterers [1]. For larger RUMs this assumption may no longer be valid and the off-diagonal terms will depend on the distance between the scatterers.

The system of observation equations can be solved with at least three sets of LoS observations, under the condition that they are spatio-temporally coinciding and independent (STCI, discussed in Sec. III-A). The row for the first set in the design matrix A is the projection of the 3D displacements onto the LoS vectors towards the first satellite position, cf. Eq. (1). We assume that for observations within one set, the angles θ and α_d are constant within the RUM.

When $m \geq 3$, the unknown displacement parameters in vector x can be estimated using direct inversion or Best Linear Unbiased Estimation [14], i.e.,

$$\hat{\underline{x}} = \begin{cases} A^{-1}\underline{y}, & \text{for } m = 3, \text{ and} \\ Q_{\hat{x}} A^T Q_y^{-1} \underline{y} & \text{for } m > 3, \text{ with} \end{cases} \tag{6}$$

$$Q_{\hat{x}} = \begin{cases} A^{-1} Q_y A^{-1}, & \text{for } m = 3, \text{ and} \\ (A^T Q_y^{-1} A)^{-1} & \text{for } m > 3. \end{cases} \tag{7}$$

For a successful estimation of the unknown displacement parameters this approach needs to satisfy several conditions,

which are discussed below.[3]

A. Spatio-temporally coinciding independent (STCI) LoS observations

The mathematical expression of Eq. (6) is only valid if all LoS observation sets from different viewing geometries are unambiguously linked to the same physical displacement signal, x. In this context, we introduce the condition of *spatio-temporally coinciding* and *independent* (STCI) LoS observations, i.e., (i) the same scatterers, from (ii) an object that is not subject to internal deformation, are observed (iii) simultaneously and (iv) from sufficiently different viewing geometries.

Obviously, the STCI condition is never fulfilled for a single target, since point scatterers (PS) observed from one orbital viewing geometry typically do not coincide with PS from another viewing geometry, apart from, e.g., lamp posts [15] or integrated geodetic reference stations (IGRS) [16]. Moreover, scatterers close to each other are not necessarily stemming from the same object, considering, e.g., a scatterer on the roof of a house and a scatterer nearby on the street, which may represent different deformation phenomena [17]. Added to this, different (parts of) objects can show different deformation phenomena [18], [19]. Finally, SAR acquisitions from different viewing geometries are never taken at the same moment, and since deformation phenomena, by definition, change over time this will result in incomparable displacement parameters. Especially for rapidly changing deformation phenomena such as landslides [20] or highly dynamic soils [21], it may be impossible to assume that observations from different epochs are comparable.

Consequently, as the strict STCI condition can never be met, the success of a decomposition is highly dependent on relaxing this conditions using additional assumptions.

B. Region of Uniform Motion

A plausible assumption that can relax the STCI condition follows from identifying *Regions of Uniform Motion* (RUMs), defined such that points that fall within a single RUM behave uniformly, driven by the same deformation phenomenon. Thus, only after defining a RUM (and aligning the different data sets in time) it will be possible to decompose the LoS observations into the unknown displacements parameters. In many cases, defining a RUM can be difficult, since it can easily contain scatterers that represent different deformation phenomena [17].

C. Datum connection

LoS observations from different observational sets should be referenced to the same spatio-temporal datum, i.e., the same spatial reference point and the same temporal reference epoch. Commonly, different viewing geometries will result in different spatial reference points. Therefore, it is at least required that the reference points of different viewing geometries represent the same deformation phenomenon i.e., the same RUM. Temporally, the selected reference SAR acquisitions, per stack, need to be aligned to refer to the same displacement parameters, x, in Eq. (6). Spatial or temporal interpolation may be required for this purpose. For displacement signals which are rapidly changing between epochs this interpolation will be more influential.

D. Full rank system

To unambiguously solve for the three unknown displacement components we require at least three sets of (STCI) observations from different viewing geometries to assure a full rank system, and consequently a unique solution. We define the *solution space* as the space that contains all possible solutions of the linear system. With only one LoS observation set, the solution space is a *solution plane* orthogonal to the LoS displacement vector that contains the end-point of the LoS displacement vector. All points located in this plane are a possible solution to the inverse problem. The orientation of the solution plane is thus completely defined by the LoS unit vector, $\mathrm{u}_{\mathrm{LoS}}$, see Eq. (3), as it is normal to the solution plane. The plane contains the end point of the LoS vector, see Eq. (2).

The equation of the solution plane with unit vector $\mathrm{u}_{\mathrm{LoS}}$ through the point $d_{\mathrm{LoS}}\,\mathrm{u}_{\mathrm{LoS}}$ is

$$\mathrm{u}_{\mathrm{LoS}} \cdot (d_{\mathrm{ENU}} - d_{\mathrm{LoS}}\mathrm{u}_{\mathrm{LoS}}) = 0, \tag{8}$$

with $d_{\mathrm{ENU}} = [d_e, d_n, d_u]^T$, $\mathrm{u}_{\mathrm{LoS}} = [\mathrm{u}_1, \mathrm{u}_2, \mathrm{u}_3]^T$, cf. Eq. (3).

When two LoS observation sets are available, the solution space reduces to a line, i.e., the intersection of the two solution planes. All points on the *solution line* are a potential solution to the inverse problem, since the line contains the endpoint of the unknown displacement vector.

To solve unambiguously for the 3D displacement vector, albeit with various degrees of precision, three or more sets of LoS observations are required. Only then, there is one unique point where the three solution planes intersect. The quality of the displacement estimator $\underline{\hat{x}}$, see Eqs. (6) and (7), follows from error propagation as

$$Q_{\hat{x}} = (A^T Q_y^{-1} A)^{-1} = \begin{bmatrix} \sigma_e^2 & \sigma_{en} & \sigma_{eu} \\ \sigma_{en} & \sigma_n^2 & \sigma_{nu} \\ \sigma_{eu} & \sigma_{nu} & \sigma_u^2 \end{bmatrix}. \tag{9}$$

The diagonal elements of $Q_{\hat{x}}$ give the variances for $\hat{d}_e$, $\hat{d}_n$, and $\hat{d}_u$ respectively. The requirement of working with three STCI LoS observation sets, stemming from the same RUM is a *necessary but insufficient* requirement. The three STCI LoS observation sets also need to have sufficiently different angular diversity to ensure full rank.

E. Angular diversity

As almost all SAR satellites operate right-looking, orbiting the Earth in near-polar retrograde orbits, they all have very similar viewing geometries, resulting in limited angular diversity. Thus, the solution lines for each combination of any ascending and descending viewing geometry will have very

[3]Within this work we focus on the decomposition of interferometric LoS observations, i.e., we do not consider adding pixel offset tracking or GNSS observations.

TABLE I
CHARACTERISTICS OF THE SIMULATED VIEWING GEOMETRIES

	Geometry type	Incidence angle θ	Azimuth ZDP α_d
A1	ascending-1	30°	260°
A2	ascending-2	41°	261°
D1	descending-1	44°	100°

similar orientations. Consequently, even with LoS observations from three viewing geometries, the inverse problem is often ill-posed [13], A is close to rank deficient, and the solution is unstable: a small difference in the LoS observations may lead to a large change in the estimated displacement components [6], [10]. This follows from the variance-covariance matrix, $Q_{\hat{x}}$, of the estimated displacement components, see Fig. 5.

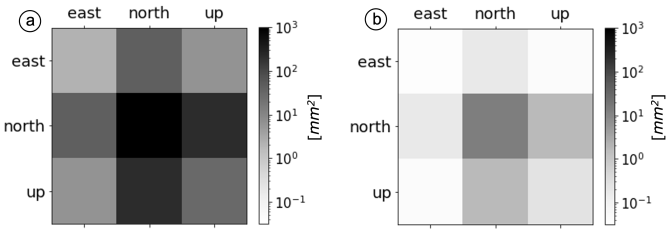

Fig. 5. Full variance-covariance matrix, $Q_{\hat{x}}$, see Eq. (9), of the estimates of the three displacement components, on a logarithmic scale. a) All observations from right-looking satellites, see Tab. I. b) Two right-looking and one left-looking satellite. This yields a significant improvement in the estimate of d_n, but also the other displacement components benefit from the addition of a left-looking radar acquisition.

Simulating three different viewing geometries, e.g., one descending and two ascending acquisitions, we compute the precision for the estimated displacement parameters using Eq. (9). Simulating one scatterer per viewing geometry (Tab. I) and using $\sigma^2_{\text{LoS}} = 1$ mm^2 for all three observations, we estimate $Q_{\hat{x}}$, see Fig. 5a. The diagonal of $Q_{\hat{x}}$ shows the variances of $\hat{d}_e$, $\hat{d}_n$, and $\hat{d}_u$. The precision (σ) with which we can estimate the north component is ∼40 times larger than the simulated σ_{LoS} values. The precisions for the east and up components are much better, i.e., 1.5 mm and 5.5 mm, respectively.

One solution to improve d_n is to add a left-looking observation as suggested by [6] and [10].[4] Fig. 5b shows $Q_{\hat{x}}$ for a situation where the second ascending acquisition is left looking. The precisions of the unknown parameters are now 0.3, 4.5, and 0.7 mm for d_e, d_n, and d_u respectively, which is about one order of magnitude improvement for all components. Nevertheless, σ_n is still the largest, especially considering that σ_{LoS} was 1 mm. Other options to retrieve d_n include using non-interferometric observables, such as along-track offset measurements [5], which are only feasible for smooth wide-area phenomena and large displacements, not for PS in the built environment with millimeter displacements. Finally, future multistatic squinted systems may also enable more variety in viewing geometry, see [23].

[4]Left-looking geometries will be feasible with the NISAR mission [22].

IV. THE NULL LINE

In many practical situations, the maximum number of STCI LoS sets is two (ascending and descending). This results in an underdetermined problem with an infinite number of possible solutions. However, when the viewing geometry of the two available acquisitions is known (i.e., before we need to have actual observations) we can define the *null line*, n, which is the null space of the projection matrix A i.e. the solution to $A\, d_{\text{ENU}} = 0$. The null line is visualized in Fig. 6, where the blue and green arrows are the LoS unit vectors corresponding to an ascending and a descending acquisition, the blue and green planes are the null planes, and the orange line is the null line.

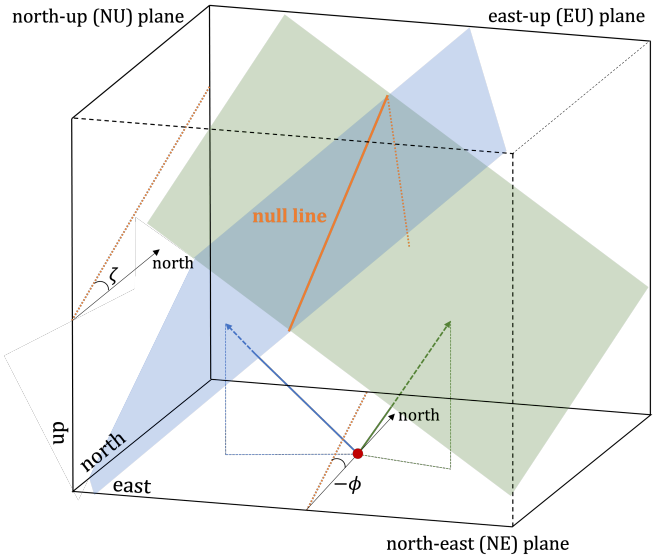

Fig. 6. When two LoS viewing geometries are available, the null line can be defined (i.e., the null space of the corresponding projection matrix). The orientation of the null line is defined as the intersection of the two null planes of the two available LoS vectors. Here we visualized one ascending (blue) and one descending (green) unit vector, and corresponding null planes. The null line is fully described by azimuth angle ϕ and elevation angle ζ since the position is irrelevant.

The orientation of the null line is an important metric for InSAR interpretation since we cannot, interferometrically, observe any displacement component in its direction i.e., both of the two viewing geometries have zero sensitivity in the direction of the null line. This direction is therefore valuable to know, before starting an InSAR survey as well as accompanying InSAR results. The null line is described by azimuth angle ϕ and elevation angle ζ. When the viewing geometry for each acquisition is known, the orientation of the null line can be computed from the cross product of the two normal vectors of the null planes (the LoS unit vectors):

$$
\begin{aligned}
n &= \mathbf{u}^{(1)}_{\text{LoS}} \times \mathbf{u}^{(2)}_{\text{LoS}} \\
&= \begin{bmatrix} \sin\theta_1 \sin\theta_2 \cos\alpha_{d,1} - \sin\theta_2 \cos\theta_1 \cos\alpha_{d,2} \\ -\sin\theta_1 \cos\theta_2 \sin\alpha_{d,1} + \sin\theta_2 \cos\theta_1 \sin\alpha_{d,2} \\ \sin\theta_1 \sin\theta_2 \sin(\alpha_{d,1} - \alpha_{d,2}) \end{bmatrix}
\end{aligned} \tag{10}
$$

where $(\theta_1, \alpha_{d,1})$ and $(\theta_2, \alpha_{d,2})$ correspond to the first and the second viewing geometry, respectively. With n it is possible to compute ϕ and ζ:

$$\phi = \tan^{-1}\left(\frac{n_1}{n_2}\right), \text{ and } \zeta = \tan^{-1}\left((\frac{n_3}{\sqrt{n_1^2+n_2^2}}\right), \quad (11)$$

where n_1, n_2, and n_3 are the east, north, and up component of n respectively.

A. Null line orientation evaluation

To evaluate the orientation of the null line for an actual mission at an arbitrary position on Earth, we apply Eq. (11) to the Sentinel-1 viewing geometry, see Figs. 7a and b.[5] This shows the values for ϕ and ζ, respectively the azimuth and elevation of the null line. We find that $\phi \approx 0°$ for the Northern Hemisphere, but that this is not always the case for the Southern Hemisphere. Moreover, everywhere on Earth the elevation angle $\zeta > 0°$.

At higher latitudes, different tracks overlap, enabling multiple ascending and descending viewing geometries per location. Therefore, Figs. 7a and b use the largest possible α_d per location, i.e., favorably the largest asymmetry between the two viewing geometries.

To investigate whether $\phi = 0°$ can really be considered a 'rule of thumb' for the Northern Hemisphere for Sentinel-1, we compute ϕ and ζ for all possible combinations between ascending and descending acquisitions for latitudes varying between $-75°$ and $+85°$, at arbitrary longitude 30°, see Figs. 7c and d. Typically for the Northern Hemisphere, all combinations result in $\phi \approx 0°$. Yet, for the higher southern latitudes, different combinations result in $\phi \neq 0°$, e.g., for applications in Antarctica. Elevation angles ζ increase significantly at higher latitudes, affecting the Arctic, South America, South Africa, New Zealand, and the Antarctic.

B. Impact of the null line orientation

Frequently[6] it is postulated that with the current orbits and viewing geometries of SAR missions, there is no sensitivity for displacement components in the north direction, and that it is therefore possible to simply 'remove' or 'disregard' d_n from the inverse problem, cf. Eq. (4), resulting in

$$E\{\underbrace{\begin{bmatrix} \underline{d}_{\text{LoS}}^{(1)} \\ \underline{d}_{\text{LoS}}^{(2)} \\ \vdots \\ \underline{d}_{\text{LoS}}^{(m)} \end{bmatrix}}_{\underline{y}}\} = \underbrace{\begin{bmatrix} \sin\theta_1 & \sin\alpha_{d,1} & \cos\theta_1 \\ \sin\theta_2 & \sin\alpha_{d,2} & \cos\theta_2 \\ \vdots & & \vdots \\ \sin\theta_m & \sin\alpha_{d,m} & \cos\theta_m \end{bmatrix}}_{A} \underbrace{\begin{bmatrix} d_e \\ d_u \end{bmatrix}}_{x}. \quad (12)$$

This would only be a valid approach when the orientation of the null line is $\phi = 0° \wedge \zeta = 0°$. However, even while ϕ may be close to zero, ζ never is. Fig. 5 reveals that the estimators for d_e, d_n and d_u are correlated. Therefore, removing d_n from the inverse problem will result in biased estimates for d_e and d_u, i.e.,

$$\begin{aligned} \hat{d}_e &= d_e + B_e, \text{ with } B_e = \tan\phi \; d_n \\ \hat{d}_u &= d_u + B_u, \text{ with } B_u = \tan\zeta \; d_n, \end{aligned} \quad (13)$$

where B_e and B_u are the biases on the estimated east and up component, respectively. The bias terms are thus the product of the (i) the orientation of the null line n, and (ii) the magnitude of the actual (but unknown) north displacement. In Tab. II we show the values for $\tan\phi$ and $\tan\zeta$ for different cities in the world. E.g., for Melbourne a 1 unit north displacement leads to a bias in the east and up component of 0.01 and 0.13 units, respectively. These values are near-identical to the azimuth ϕ and elevation ζ angles, when expressed in radians, see Fig. 7

Geometrically, removing d_n from the decomposition equation is equivalent to projecting both LoS observations onto the east-up (EU) plane.[7] Thus, also the 3D null line will be projected onto the EU plane, which yields a line that we refer to as k, see Fig. 8. Line k has elevation angle ξ, and as long as $\xi \neq 90°$ and $\xi \neq 0°$, k has both a component in the up and east direction, i.e., k contains infinitely many combinations of d_e and d_u. Consequently, it is not possible to give unbiased estimates for both d_e and d_n. If and only if $\phi = 0°$, line k has no component in the east direction and $\xi = 90°$, yielding an unbiased d_e and a biased d_u component.

TABLE II
SCALING FACTORS FOR THE BIAS IN THE EAST AND UP DIRECTION FOR DIFFERENT CITIES IN THE WORLD, INDICATING THAT A NON-ZERO NORTH COMPONENT MULTIPLIED BY THE GIVEN NUMBER WILL YIELD THE BIAS IN THE EAST AND UP COMPONENT, RESPECTIVELY, SEE EQ. (13).

City	East ($\tan\phi$)	Up ($\tan\zeta$)
London	0.01	0.09
New York	0.01	0.08
Los Angeles	0.01	0.08
Melbourne	0.01	0.13
Svalbard	0	0.16
Antartic Peninsula	0.05	0.22
Singapore	0.01	0.10

C. The null line aligned (NLA) frame

Using the concept of the null line with its unique orientation in 3D space, we propose a *null line aligned* (NLA) coordinate system with the first axis in the local horizontal plane, the second axis aligned along the null line, and the third one complementing the right-handed 3D Cartesian system, see Fig. 8c.

The plane orthogonal to the null line (i.e., spanned by the first and third axes) is termed the NLA-plane and has the unique characteristic that an orthogonal projection of any displacement vector onto that plane will not influence (bias) the two in-plane components. This characteristic of unbiasedness makes the NLA system optimally suited for direct usage in mathematical or geophysical models, as opposed to the frequently-used[8] east-up (EU) plane, which is biased by

[5]The software that computes the orientation of the null line for different satellite missions at different locations on Earth, is made available via [24].

[6]e.g., [25], [26], [27], [28], [29], [30], [31], [32], [33], [34], [35]

[7]Note that this is a *discretionary* projection, and not a *forced* projection, as introduced in Sec. II-B.

[8]e.g., [36], [26], [33], [28], [29]

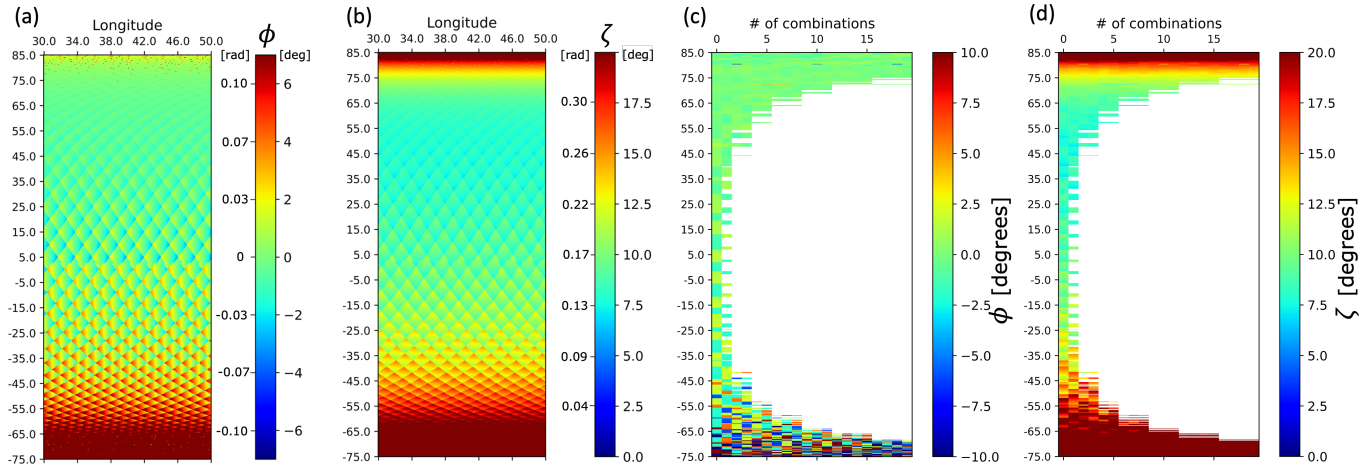

Fig. 7. Orientation of the null line for Sentinel-1, defined by ϕ and ζ, see Fig. 6. The checkered pattern is due to the S1 orbit pattern. (a): azimuth ϕ, (b): elevation ζ. Values are calculated by combining the ascending and descending observations that have a maximum azimuth of the ZDP, for each location on Earth, considering the maximum asymmetry between the two ZDP's. This demonstrates that $\phi \approx 0°$ for the Northern Hemisphere. The values for ϕ and ζ in radians are near-identical to the $\tan\phi$ and $\tan\zeta$ factors in Eq. (13), for the east- and up-bias, respectively. (c) and (d), ϕ and ζ values for all possible combinations between overlapping ascending and descending acquisitions. Results computed using [24].

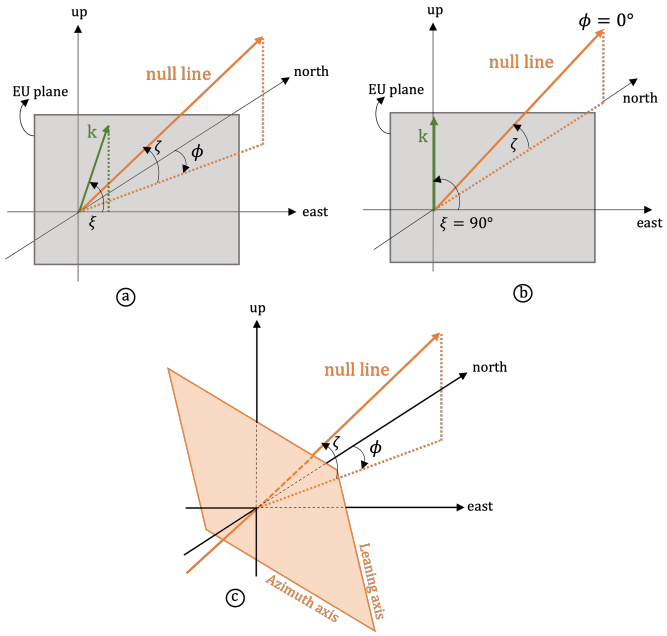

Fig. 8. The orientation of the null line n in the ENU reference frame is given by azimuth angle ϕ and elevation angle ζ. The projection of n onto the east-up (EU) plane is line k which has elevation angle ξ. In (a), $\phi \neq 0°$ and $\zeta \neq 0°$ and therefore k as a component in the east and up direction, i.e., $\xi \neq 90°$. In (b), $\phi = 0°$ and therefore $\xi = 90°$, k only has a component in the up direction. In (c) we show the orientation of the NLA frame with the plane spanned by the Leaning axis (with elevation angle $\zeta + 90°$) and Azimuth axis (with azimuth $\phi + 90°$) in orange. The null line is orthogonal to this plane.

definition. Obviously, intuitive interpretability of NLA results and visualizations may require some training.

Using the NLA acronym as mnemonic, the axes can be referred to as the *N*ull-line (axis), the *L*eaning axis, which is tilted backward with an elevation angle of $\zeta + 90°$, and the *A*zimuth axis, which is horizontal with azimuth $\phi + 90°$, see also Fig. 8c.

Projecting the two LoS observation vectors independently onto the NLA-plane allows for the simple (and unbiased) retrieval of the resultant vector.

V. Evaluation of Current Practice

While the geometry of InSAR follows from conventional linear algebra, its application in practice is conditional to assumptions and requires strict adherence to the conditions formulated in Sec. III. Evaluating contemporary literature on InSAR geometry shows that this is not always the case. We identify three types of typical geometric flaws in InSAR, related to attribution, projection, and decomposition.

A. Attribution

Attribution errors occur when the line-of-sight observation is literally attributed to one displacement direction (usually the vertical), given only a single viewing geometry, without projection and without further justification. Obviously, this is erroneous, and results in a severe underestimation (bias) of vertical displacements of $(\cos\theta)^{-1}$, i.e., up to 40%, see Eq. (1). While explicit attribution errors were more common in the early days of InSAR, ambiguous statements or colorbar labels can still be found in recent literature and products.[9] Moreover, describing LoS motion with words such as 'subsidence' adds another layer of semantic confusion.[10] Attribution errors can be easily avoided by explicitly stating prior assumptions and using unambiguous axes and colorbar labels.

B. Projection

Projection errors occur, e.g., when LoS displacement estimates are actually '*projected onto the vertical*,' (PoV) but

[9] e.g., [37], [38], [39], [40], [41]
[10] e.g., [40], [42]

are subsequently presented as '*vertical displacements*'. Obviously, these two estimates would only be identical under the assumption that any non-vertical displacement component of the 3D displacement vector is zero. Since this assumption is in many cases incorrect, e.g., for landslides, but even for subsidence bowls, it leads to a biased estimate. Such a bias can have a significant impact combined with a small likelihood of being detected.[11] Often, explicit assumptions on the non-existence of the horizontal component are lacking.[12] Typically, projection errors go hand in hand with indistinct verbs, such as 'converted', 'transformed', 'computed', 'calculated', or 'determined'. These all suggest that there is a unique relation between the LoS displacements and the vertical displacements, which is in general incorrect.

C. Decomposition

The most frequently occurring geometric InSAR fallacy is a *decomposition error*, which occurs when the existence of a null space is ignored, see Sec. IV. A typical example of a decomposition error is the suggestion that *by combining an ascending and a descending time-series, it is possible to disentangle east-west horizontal deformation from vertical deformation.*[13] Statements such as these have in common that they suggest that it is possible to unambiguously and unbiasedly 'disentangle', 'estimate', 'determine', 'compute', or 'reconstruct' two displacements components, usually the vertical and east component, with two LoS observations. As discussed in Sec. IV-B, with these viewing geometries this will always result in biased estimates, except for the NLA coordinate system proposed in Sec. IV-C. Consequently, also a decomposition into the plane spanned by the up direction and the azimuth look direction of one of the satellites is incorrect (i.e., biased) since this plane is not orthogonal to the null line.

Two variations on decomposition errors can be distinguished.

1) Assuming signal-sensitivity dependency: The first variant of a decomposition error occurs when it is assumed that due to the *lack of sensitivity* for the north-component, d_n, it can be removed from the inverse problem altogether.[14] This assumption would only be valid if the orientation of the null line n is $(\phi, \zeta) = (0, 0)$, hence in the north and horizontal direction respectively, which is never the case, see Fig. 7. Thus, removing d_n from Eq. (4) cannot be justified by the low sensitivity for that component unless we have prior knowledge of the expected magnitude of the north-component. When d_n is larger than the noise level of the projected LoS observations, it can still be discriminated from the observations.

2) Assuming displacement components to be known: The second variant of a decomposition error occurs when it is argued that $d_n = 0$ as a consequence of the insensitivity to displacements into the north direction.[15][16] Obviously, this assumption refers to the actual size of the physical signal, i.e., the unknown parameter, which is evidently not correlated to the sensitivity of a particular radar instrument. The flawed argument is made in order to reduce the number of unknowns from three to two, and subsequently arrive at a square linear system.

In conclusion, the implicit assumption that with two observation geometries we can estimate any arbitrary two directions in 3D space (including the fashionable EU decomposition), by deliberately ignoring d_n, or by assuming that d_n is known, leads to an erroneous (i.e., biased) decomposition.

VI. Recommendations for InSAR product generation and interpretation

While the underdetermined nature of the problem cannot be formally solved, we propose to pursue standardization for InSAR product generation and interpretation. First, we discuss two options for performing a displacement vector *decomposition* given two viewing geometries. Then, we evaluate the options for displacement vector *projection* onto a 1D direction and a 2D plane.

A. Recommendations for vector decomposition

A decomposition of two LoS observations is feasible when the two LoS observations are STCI. Yet, as this is practically impossible (Section III-A), it is necessary to define a RUM, and perform a datum connection, see Section III. Given the model of observation equations of Eqs. (4) and (5) with only two observation geometries, the only way to reduce the rank deficiency is to reduce the parameter space from three to two unknown parameters. This goal can be achieved in two ways.

The first 'physical' option is to change the orientation of the Cartesian reference frame in combination with a priori physical information: the *strap-down system*, which we discuss in detail in [53]. For example, for many physical phenomena gravity is the driving force for displacements, which allows us to define a two-dimensional vertical plane in which the displacement vector is expected to be situated. Examples include landslides and glaciers, where this plane is spanned by the vector normal to the slope and the gravity vector [54], [55], [56], [20], or for line infrastructure where it may be assumed that no displacements occur in its longitudinal direction [57], [58]. Both require a known rotation of the Cartesian frame such that one direction can be plausibly assumed to be displacement-free. Consequently, any frame misalignment will result in biased estimates, see Section IV.

A second 'geometric' option is to take advantage of the orientation of the null space, by choosing a *null line aligned* (NLA) Cartesian coordinate system, see Section IV-C. This yields a plane orthogonal to the null line, and the (forced) orthogonal projection of a displacement vector onto that plane

[11] e.g., [43], [44], [45], [46], [47]
[12] e.g., [48], [49], [50], [51]
[13] e.g., [26], [33], [28], [29]
[14] e.g., [25], [26], [27], [28], [29], [30], [31], [32], [33], [34], [35], [52].

[15] e.g., [33], [30], [34]. Note that the $d_n = 0$ assumption is a specific case of the more generic assumption that d_n is known.
[16] Note the subtle difference between variant 1, which simply removes the d_n component, and variant 2, which assumes it is equal to a known value, i.e., zero.

will not influence (bias) the two in-plane components. Thus, these in-plane components can be uniquely and unbiasedly estimated. This option is particularly recommended when the InSAR results are used as input in a physical or mathematical model, since their unbiased nature will not compromise the output of that model.

For both the 'physical' as well as the 'geometrical' option, we recommend to explicitly mention the orientation of the null line with the InSAR product since it comprises information on the direction in which displacements cannot be observed.

Frequently-used alternative options are not recommended. Theoretically, when it would be known from physics that a displacement component is zero in a cardinal compass direction, i.e., a northbound component equal to zero ($d_n = 0$), the parameter space has dimension two, and the remaining parameters may be uniquely estimated. However, while this physics-based rank-reduction may not be impossible, e.g. considering perfectly east-west oriented tectonic faults [6], it is a solution that is in a generic sense physically unrealistic and often unsubstantiated, since dynamic processes on earth typically do not have a preference for a cardinal compass direction. Likewise, it is not recommended to use the widely advocated and applied decomposition in the EU-plane, as this introduces biases, is prone to misinterpretation, and suggests an estimation possibility that is non-existent, see Section IV-B.

B. Recommendations for vector projection

When there is no deformation direction in which displacements are known to be zero, or when it is inconvenient to decompose the two LoS observations in the plane orthogonal to the null line, it will not be possible to *decompose* the LoS observations. Yet, a *projection* is an operation that that is admissible and can always be performed without exceptions or assumptions. Clearly, a projection product is different from *estimating* the unknown parameter in the corresponding direction. Moreover, 'projection-onto' products are *discretionary* projections, and it is up to the user to decide on whether such a projection contains intelligible information. We distinguish *projection* onto a 1D direction from a single viewing geometry, and onto a 2D plane from dual viewing geometries.

1) Projecting one LoS observation onto one direction: With only one LoS observation available, it is possible to project that observation onto any particular direction. For example, often d_{LoS} is projected onto the vertical (PoV) direction using

$$d_{\text{PoV}} = P_{\text{up, LoS}^\perp}\, d_{\text{LoS}} = (\cos\theta)^{-1} d_{\text{LoS}}, \tag{14}$$

where $P_{\text{up, LoS}^\perp}$ is the projector, and d_{PoV} is the projection of d_{LoS} onto the vertical direction. Note that in general $d_{\text{PoV}} \neq d_{\text{up}}$. The operation is an *oblique* projection of the LoS observations onto the vertical axis, along a plane orthogonal to the LoS unit vector. In contrast, when the LoS observations would be projected *orthogonally* onto the vertical, i.e., along a plane orthogonal to the 'up' unit vector, that would result in

$$d_{\text{PoV}^\perp} = P_{\text{up, up}^\perp} d_{\text{LoS}} = \underbrace{\begin{bmatrix} 0 & 0 & 0 \\ 0 & 0 & 0 \\ 0 & 0 & 1 \end{bmatrix}}_{P} \mathrm{u}_{\text{LoS}} d_{\text{LoS}} = \cos\theta\, d_{\text{LoS}}, \tag{15}$$

Thus, both $P_{\text{up, LoS}^\perp}$ and $P_{\text{up, up}^\perp}$ are allowable discretionary projectors, but with a different result.

The main recommendation is therefore to (i) explicitly mention the use of a *projection-onto* product, e.g. using the PoV as subscript similar to the LoS subscript, and (ii) explicitly distinguish an oblique from an orthogonal projection, using the $\perp$ indicator. This is necessary both in text as well as in cartographic symbols and, e.g., colorbar annotations. Furthermore, we recommend to report the orientation of the null plane, since it is the plane where no displacements can be observed.

2) Projecting two LoS observations onto a plane: When two LoS observations are available, the observations can be projected onto any arbitrary plane. When a LoS displacement vector is projected onto the plane spanned by the east and up axis, i.e., the EU plane, we have

$$d_{\text{PoEU}} = \underbrace{\begin{bmatrix} 1 & 0 & 0 \\ 0 & 0 & 0 \\ 0 & 0 & 1 \end{bmatrix}}_{P} \mathrm{u}_{\text{LoS}} d_{\text{LoS}}, \tag{16}$$

where d_{PoEU} is the projection of d_{LoS} onto the EU plane. When this projection is performed for the two LoS observations it is possible to transform the projections into east and up components with Eq. (12) resulting in $d_{e,\text{PoEU}}$ and $d_{u,\text{PoEU}}$. However, it should be stressed that the results $(d_{e,\text{PoEU}}, d_{u,\text{PoEU}})$, are not the same as the unknown displacement components (d_e, d_u).

C. Presenting LoS observations unaltered

The last option for handling the underdeterminedness problem is presenting the LoS observations unaltered as the final product. This is obviously correct, as it does not attempt to do any projection, attribution, or decomposition, as in [25], [59], [60], [61]. The drawback of the LoS product is that it is typically more difficult to interpret, especially for non-experts. As the actual vertical and horizontal displacement components are projected onto the LoS and superposed, what happens in the real world remains obscured. Yet, this is the preferred option when the InSAR results are used as input in a physical or mathematical model, since their unbiased nature will not compromise the output of that model.

VII. Conclusions

Based on a general review of InSAR geometry, including the geometry-defining parameters from the satellite orbits in combination with the curved earth, the relationship between the LoS observables and the 3D displacement components is described. Whether decomposition—i.e., estimation of (some of the) 3D displacement parameters—is permitted is dependent

on the **STCI** condition: spatio-temporally coinciding independent observations. As this condition is typically never fulfilled, it can be relaxed using the explicit assumption of **RUM**s: regions of uniform motion. Together with explicit spatio-temporal datum connection between the SAR datasets and $\leq$3 (full rank) viewing geometries with sufficient angular diversity, the quality of the estimates can be derived. In many practical situations, at most two viewing geometries are available, defining the **null line**, whose orientation defines the estimability of displacement components. It depends on the orbital and viewing geometry as well as on the location on earth. The null line orientation should be stated explicitly in any standard InSAR product, as it is one of the fundamental metrics required for a proper interpretation. The null line also allows for the definition of the only unbiased reference system for displacement component estimation without without necessarily adding assumptions, termed **NLA**: the null-line aligned coordinate system.

Evaluating current practice yields three types of errors that are frequently encountered: which are termed attribution, projection, and decomposition errors. These lead to recommendations for InSAR product generation and interpretation. For vector decomposition, it is recommended to use the strap-down or the null-line aligned coordinate system, to prevent biased estimation, and refrain from using the biased decomposition on the East-Up plane. For vector projections, it is recommended to use descriptive subscripts, d_{LoS}, d_{PoV}, $d_{\mathrm{PoV}^{\perp}}$, or d_{PoEU} to unambiguously define projected InSAR products, both textual as well as in maps and graphs.

The code to compute the null line orientation for any arbitrary location on Earth is available for download via https://gitlab.tudelft.nl/drama/drama [24].

ACKNOWLEDGMENT

We would like to thank Dr. F. van Leijen and two anonymous reviewers for their valuable comments.

REFERENCES

[1] R. F. Hanssen, *Radar Interferometry: Data Interpretation and Error Analysis*. Dordrecht: Kluwer Academic Publishers, 2001.

[2] D. Massonnet, M. Rossi, C. Carmona, F. Adagna, G. Peltzer, K. Feigl, and T. Rabaute, "The displacement field of the Landers earthquake mapped by radar interferometry," *Nature*, vol. 364, no. 8, pp. 138–142, Jul.-8 1993.

[3] H. A. Zebker, P. A. Rosen, R. M. Goldstein, A. Gabriel, and C. L. Werner, "On the derivation of coseismic displacement fields using differential radar interferometry: The Landers earthquake," *J. Geophys. Res.*, vol. 99, no. B10, pp. 19 617–19 634, Oct.-10 1994.

[4] D. Massonnet and K. L. Feigl, "Satellite radar interferometric map of the coseismic deformation field of the M = 6.1 Eureka Valley, California earthquake of May 17, 1993," *Geophys. Res. Lett.*, vol. 22, no. 12, pp. 1541–1544, 1995.

[5] Y. Fialko, M. Simons, and D. Agnew, "The complete (3-D) surface displacement field in the epicentral area of the 1999 mw 7.1 Hector Mine earthquake, California, from space geodetic observations," *Geophys. Res. Lett.*, vol. 28, no. 16, p. 3063, 2001.

[6] T. J. Wright, B. E. Parsons, and Z. Lu, "Towards mapping surface deformation in three dimensions using InSAR," *Geophys. Res. Lett.*, vol. 31, p. 5 pp., 2004.

[7] J. Hu, Z. Li, X. Ding, J. Zhu, L. Zhang, and Q. Sun, "Resolving three-dimensional surface displacements from InSAR measurements: A review," *Earth Sci Rev*, vol. 133, pp. 1–17, 2014.

[8] T. Fuhrmann and M. C. Garthwaite, "Resolving three-dimensional surface motion with InSAR: Constraints from multi-geometry data fusion," *Remote Sens.*, vol. 11, no. 3, p. 241, 2019.

[9] G. Strang, *Linear algebra and its applications*, 3rd ed. Fort Worth: Harcourt Brace Jovanovich College Publishers, 1988.

[10] F. Rocca, "3D motion recovery with multi-angle and/or left right interferometry," in *Proc. of the third Int. Workshop on ERS SAR*, 2003.

[11] European Space Agency. (2021) Sentinel 1 SAR Acquisition Modes. [Online]. Available: https://sentinels.copernicus.eu/web/sentinel/user-guides/sentinel-1-sar/acquisition-modes/interferometric-wide-swath

[12] P. Lopez-Dekker and A. Theodosiou. (2022) DRaMA software. [Online]. Available: https://gitlab.tudelft.nl/drama/drama

[13] A. Tarantola, *Inverse Problems Theory*. New York: Elsevier, 1987.

[14] P. J. G. Teunissen, *Adjustment theory; an introduction*, 1st ed. Delft: Delft University Press, 2000.

[15] X. X. Zhu, S. Montazeri, C. Gisinger, R. F. Hanssen, and R. Bamler, "Geodetic SAR tomography," *IEEE Trans. on Geosci. and Remote Sens.*, vol. 54, no. 1, pp. 18–35, 2015.

[16] R. F. Hanssen, "A radar retroreflector device and a method of preparing a radar retroflector device," patent, 12 27, 2018.

[17] V. B. H. Ketelaar, *Monitoring surface deformation induced by hydrocarbon production using satellite radar interferometry*. Springer, 2008.

[18] P. Dheenathayalan, D. Small, A. Schubert, and R. F. Hanssen, "High-precision positioning of radar scatterers," *J. of Geodesy*, vol. 90, no. 5, pp. 403–422, 2016.

[19] M. Yang, P. López-Dekker, P. Dheenathayalan, F. Biljecki, M. Liao, and R. F. Hanssen, "Linking persistent scatterers to the built environment using ray tracing on urban models," *IEEE Trans. Geosci. Remote Sens.*, vol. 57, no. 8, pp. 5764–5776, 2019.

[20] A. Van Natijne, T. Bogaard, F. van Leijen, R. Hanssen, and R. Lindenbergh, "World-wide insar sensitivity index for landslide deformation tracking," *Int. J. Appl. Earth Obs. Geoinf.*, vol. 111, p. 102829, 2022.

[21] P. Conroy, S. A. Van Diepen, S. Van Asselen, G. Erkens, F. J. Van Leijen, and R. F. Hanssen, "Probabilistic estimation of insar displacement phase guided by contextual information and artificial intelligence," *IEEE Trans. Geosci. Remote Sens.*, vol. 60, pp. 1–11, 2022.

[22] M. Simons, D. Bekaert, A. Borsa, A. Donnellan, E. Fielding, C. Jones, R. Lohman, Z. Lu, F. Meyer, S. Owen *et al.*, "Nisar requirements and validation approach for solid earth science," in *2021 IEEE IGARSS*. IEEE, 2021, pp. 543–546.

[23] A. Hooper, J. Biggs, P. Prats-Iraola, F. Albino, F. De Zan, A. Parizzi, M. Rodriguez-Cassola, P. Lopez-Dekker, and B. Rommen, "Harmony: science objectives and mission overview," in *ESA LPS 2022*, 2022.

[24] W. Brouwer and R. Hanssen, *No-DRaMA software*, 2022. Retrieved on: July 14, 2022, from https://gitlab.tudelft.nl/drama/drama. [Online]. Available: https://gitlab.tudelft.nl/drama/drama

[25] B. V. Yazici and E. Tunc Gormus, "Investigating persistent scatterer InSAR (PSInSAR) technique efficiency for landslides mapping: a case study in Artvin dam area, in Turkey," *Geocarto Int.*, pp. 1–19, 2020.

[26] H. Klemm, I. Quseimi, F. Novali, A. Ferretti, and A. Tamburini, "Monitoring horizontal and vertical surface deformation over a hydrocarbon reservoir by PSInSAR," *First break*, vol. 28, no. 5, 2010.

[27] A. Rucci, D. Vasco, and F. Novali, "Monitoring the geologic storage of carbon dioxide using multicomponent SAR interferometry," *Geophys. J. Int.*, vol. 193, no. 1, pp. 197–208, 2013.

[28] C. Janna, N. Castelletto, M. Ferronato, G. Gambolati, and P. Teatini, "A geomechanical transversely isotropic model of the Po river basin using PSInSAR derived horizontal displacement," *Int. J. Rock Mech. Min. Sci.*, vol. 51, pp. 105–118, 2012.

[29] S. Yun, P. Segall, and H. Zebker, "Constraints on magma chamber geometry at Sierra Negra volcano, Galápagos Islands, based on InSAR observations," *J. Volcanol. Geotherm. Res*, vol. 150, no. 1-3, pp. 232–243, 2006.

[30] K. Pawluszek-Filipiak and A. Borkowski, "Integration of DInSAR and SBAS techniques to determine mining-related deformations using Sentinel-1 data: The case study of Rydułtowy mine in Poland," *Remote Sens.*, vol. 12, no. 2, p. 242, 2020.

[31] P. Teatini, N. Castelletto, M. Ferronato, G. Gambolati, C. Janna, E. Cairo, D. Marzorati, D. Colombo, A. Ferretti, A. Bagliani *et al.*, "Geomechanical response to seasonal gas storage in depleted reservoirs: A case study in the Po river basin, Italy," *J. Geophys. Res. Earth. Surf.*, vol. 116, no. F2, 2011.

[32] A. Tamburini, M. Bianchi, C. Giannico, and F. Novali, "Retrieving surface deformation by PSInSAR™ technology: A powerful tool in reservoir monitoring," *Int. J. Greenh. Gas Control.*, vol. 4, no. 6, pp. 928–937, 2010.

[33] D. H. T. Minh, N. Yen-Nhi, T. T. Lê, T. C. Le, H. S. Bui, Q. V. Vuong, and T. Le Toan, "Quantifying horizontal and vertical movements in Ho Chi Minh city by Sentinel-1 radar interferometry," *Preprints.org*, vol. not peer-reviewed, 2021.

[34] S. Alatza, I. Papoutsis, D. Paradissis, C. Kontoes, G. A. Papadopoulos, and C. Raptakis, "InSAR time-series analysis for monitoring ground displacement trends in the western Hellenic Arc: The Kythira Island, Greece," *Geosci.*, vol. 10, no. 8, p. 293, 2020.

[35] M. Imamoglu, F. Kahraman, Z. Cakir, and F. B. Sanli, "Ground deformation analysis of Bolvadin (w. Turkey) by means of multi-temporal InSAR techniques and Sentinel-1 data," *Remote Sens.*, vol. 11, no. 9, p. 1069, 2019.

[36] M. Costantini, F. Minati, F. Trillo, A. Ferretti, E. Passera, A. Rucci, J. Dehls, Y. Larsen, P. Marinkovic, M. Eineder, R. Brcic, R. Siegmund, P. Kotzerke, A. Kenyeres, V. Costantini, S. Proietti, L. Solari, and H. S. Andersen, "EGMS: Europe-wide ground motion monitoring based on full resolution Insar processing of all Sentinel-1 acquisitions," in *IGARSS 2022 - 2022 IEEE IGARSS*, 2022, pp. 5093–5096.

[37] L. Zhou, J. Guo, J. Hu, J. Li, Y. Xu, Y. Pan, and M. Shi, "Wuhan surface subsidence analysis in 2015–2016 based on sentinel-1a data by SBAS-InSAR," *Remote Sens.*, vol. 9, no. 10, p. 982, 2017.

[38] P. Teatini, L. Tosi, T. Strozzi, L. Carbognin, U. Wegmüller, and F. Rizzetto, "Mapping regional land displacements in the Venice coastland by an integrated monitoring system," *Remote Sens. Env.*, vol. 98, no. 4, pp. 403–413, 2005.

[39] S. Stramondo, F. Bozzano, F. Marra, U. Wegmuller, F. Cinti, M. Moro, and M. Saroli, "Subsidence induced by urbanisation in the city of Rome detected by advanced InSAR technique and geotechnical investigations," *Remote Sens. Env.*, vol. 112, no. 6, pp. 3160–3172, 2008.

[40] L. Solari, A. Ciampalini, F. Raspini, S. Bianchini, and S. Moretti, "PSInSAR analysis in the Pisa urban area (Italy): a case study of subsidence related to stratigraphical factors and urbanization," *Remote Sens.*, vol. 8, no. 2, p. 120, 2016.

[41] M. Zheng, K. Deng, H. Fan, and S. Du, "Monitoring and analysis of surface deformation in mining area based on InSAR and GRACE," *Remote Sens.*, vol. 10, no. 9, p. 1392, 2018.

[42] N. Svigkas, C. Loupasakis, P. Tsangaratos, I. Papoutsis, A. Kiratzi, and C. H. Kontoes, "A deformation study of Anthemountas graben (northern Greece) based on in situ data and new InSAR results," *Arab. J. Geosci.*, vol. 13, no. 13, pp. 1–13, 2020.

[43] A. H.-M. Ng, H. Wang, Y. Dai, C. Pagli, W. Chen, L. Ge, Z. Du, and K. Zhang, "InSAR reveals land deformation at Guangzhou and Foshan, China between 2011 and 2017 with COSMO-SkyMed data," *Remote Sens.*, vol. 10, no. 6, p. 813, 2018.

[44] M. Haghshenas Haghighi and M. Motagh, "Sentinel-1 InSAR over Germany: Large-scale interferometry, atmospheric effects, and ground deformation mapping," *ZfV: Zeitschrift für Geodäsie, Geoinformation und Landmanagement*, vol. 2017, no. 4, pp. 245–256, 2017.

[45] R. Bonì, F. Cigna, S. Bricker, C. Meisina, and H. McCormack, "Characterisation of hydraulic head changes and aquifer properties in the london basin using persistent scatterer interferometry ground motion data," *J. of Hydrology*, vol. 540, pp. 835–849, 2016.

[46] W. Tang, P. Yuan, M. Liao, and T. Balz, "Investigation of ground deformation in Taiyuan Basin, China from 2003 to 2010, with atmosphere-corrected time series InSAR," *Remote Sens.*, vol. 10, no. 9, p. 1499, 2018.

[47] R. N. Nof, G. Baer, A. Ziv, E. Raz, S. Atzori, and S. Salvi, "Sinkhole precursors along the Dead Sea, Israel, revealed by SAR interferometry," *Geology*, vol. 41, no. 9, pp. 1019–1022, 2013.

[48] S. Alatza, I. Papoutsis, D. Paradissis, C. Kontoes, and G. A. Papadopoulos, "Multi-temporal insar analysis for monitoring ground deformation in amorgos island, greece," *Sensors*, vol. 20, no. 2, p. 338, 2020.

[49] N. Short, A.-M. LeBlanc, W. Sladen, G. Oldenborger, V. Mathon-Dufour, and B. Brisco, "RADARSAT-2 D-InSAR for ground displacement in permafrost terrain, validation from Iqaluit Airport, Baffin Island, Canada," *Remote Sens. Env.*, vol. 141, pp. 40–51, 2014.

[50] D. Raucoules, C. Maisons, C. Carnec, S. Le Mouelic, C. King, and S. Hosford, "Monitoring of slow ground deformation by ERS radar interferometry on the Vauvert salt mine (France): Comparison with ground-based measurement," *Remote Sens. Env.*, vol. 88, no. 4, pp. 468–478, 2003.

[51] H. Sun, Q. Zhang, C. Zhao, C. Yang, Q. Sun, and W. Chen, "Monitoring land subsidence in the southern part of the lower Liaohe plain, China with a multi-track PS-InSAR technique," *Remote sens. of environ.*, vol. 188, pp. 73–84, 2017.

[52] A. Pepe and F. Calò, "A review of interferometric synthetic aperture radar (InSAR) multi-track approaches for the retrieval of Earth's surface displacements," *Applied Sciences*, vol. 7, no. 12, p. 1264, 2017.

[53] W. Brouwer and R. Hanssen, "Estimating 3 dimensional displacements with InSAR: the strap-down solution," *under review*, vol. xx, p. xxxx, 2022.

[54] J. J. Mohr, "Repeat track SAR interferometry. an investigation of its utility for studies of glacier dynamics," Ph.D. dissertation, Technical University of Denmark, Copenhagen, May 1997.

[55] L. Cascini, G. Fornaro, and D. Peduto, "Advanced low-and full-resolution DInSAR map generation for slow-moving landslide analysis at different scales," *Engineering Geology*, vol. 112, no. 1-4, pp. 29–42, 2010.

[56] V. Greif and J. Vlcko, "Monitoring of post-failure landslide deformation by the PS-InSAR technique at Lubietova in central Slovakia," *Environ. Earth Sci.*, vol. 66, no. 6, pp. 1585–1595, 2012.

[57] I. E. Özer, F. J. van Leijen, S. N. Jonkman, and R. F. Hanssen, "Applicability of satellite radar imaging to monitor the conditions of levees," *J. of Flood Risk Management*, vol. 12, no. S2, p. e12509, 2019.

[58] L. Chang, R. P. Dollevoet, and R. F. Hanssen, "Monitoring line-infrastructure with multisensor sar interferometry: products and performance assessment metrics," *IEEE j. of selected topics in applied earth observations and remote sens.*, vol. 11, no. 5, pp. 1593–1605, 2018.

[59] N. Fatholahi, M. Akhoondzadeh, and A. Bahroudi, "An investigation of surface deformation over oilfield in southwest Iran (2003–2010) using InSAR and physical modelling," *Int. J. of Remote Sens.*, vol. 41, no. 14, pp. 5355–5370, 2020.

[60] R. Guo, L. Sumin, Y. Chen, X. Li, and L. Yuan, "Identification and monitoring landslides in longitudinal range-gorge region with InSAR fusion integrated visibility analysis," *Landslides*, pp. 1–18, 2020.

[61] L. Wang, K. Deng, and M. Zheng, "Research on ground deformation monitoring method in mining areas using the probability integral model fusion D-InSAR, sub-band InSAR and offset-tracking," *Int. J. of Applied Earth Observation and Geoinf.*, vol. 85, p. 101981, 2020.

Wietske Brouwer received the BSc degree and MSc degrees in Civil Engineering from Delft University of Technology in 2018 and 2021, respectively. She is currently pursuing her PhD degree at TU Delft, working on mathematical aspects of satellite radar interferometry.

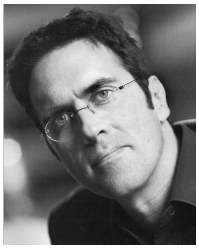

Ramon F. Hanssen (M'04-SM'15) received the M.Sc. degree in Geodetic Engineering and the Ph.D. degree (cum laude) from Delft University of Technology, The Netherlands, in 1993 and 2001, respectively.

He was with the International Institute for Aerospace Survey and Earth Science (ITC), Stuttgart University, Stuttgart, Germany; the German Aerospace Center (DLR), Weßling, Germany; Stanford University, Stanford, CA, USA, as a Fulbright Fellow; and the Scripps Institution of Oceanography, University of California at San Diego, La Jolla, CA, USA, involved in microwave remote sensing, radar interferometry, signal processing, and geophysical application development. Since 2008, he has been an Antoni van Leeuwenhoek Professor in earth observation with the Delft University of Technology, where he has been leading the research group on mathematical geodesy and positioning since 2009. He has authored a textbook on radar interferometry.